

Supplementary Figures and Tables

Inhibition of SRC prevents bone metastasis of breast cancer by blocking metastatic cell motility and bone directionality

Yong June Choi^{1,2,†}, Minju Kwon^{1,†}, Myung Jun Kim¹, Munkyung Choi¹, Phuong Thao Tran¹, Yujeong Lee¹, Wan Seob Shim¹, Minjae Kang¹, Seungseok Oh¹, Sung-Chul Lim³, Yong-Chul Kim⁴, Keon Wook Kang^{1,*}

[†]These authors contributed equally.

*Corresponding Author, E-mail: kwkang@snu.ac.kr

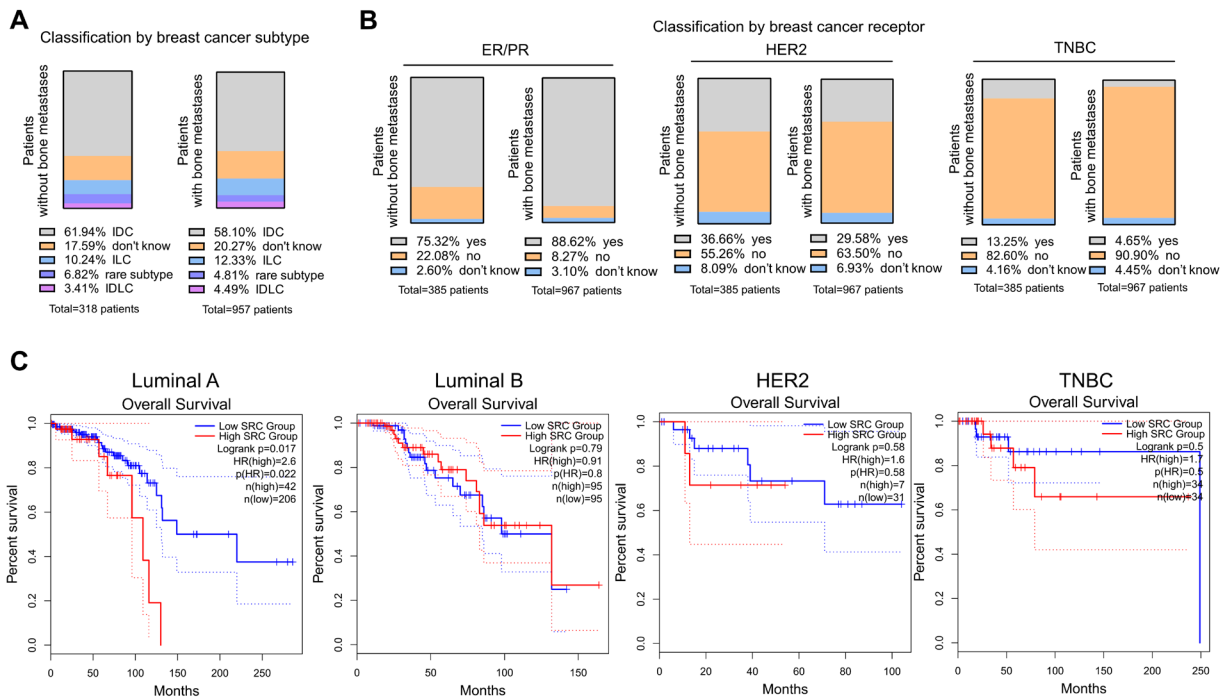


Figure S1, related to Figure 1. Distribution of breast cancer subtypes and receptor profiles in bone metastatic cohorts.

(A, B) Distribution of breast cancer subtypes in patients with and without bone metastasis. (The MBC Project, 2015–2025). (C) Survival analysis of breast cancer patients stratified by SRC expression across different subtypes. Data were obtained from the GEPIA public database. Abbreviations: IDC, invasive ductal carcinoma; ILC, invasive lobular carcinoma; IDLC, invasive ductal and lobular carcinoma.

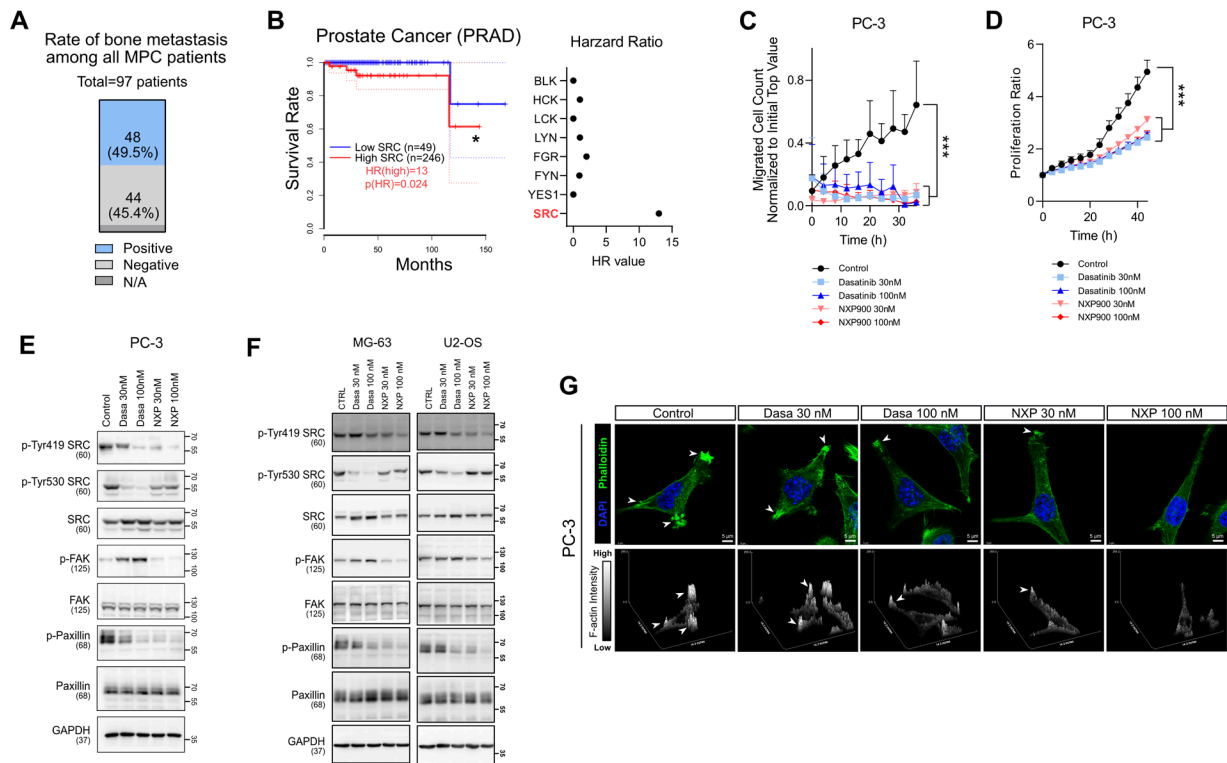


Figure S2, related to Figure 1-2. SRC contributes to cell motility and poor prognosis in prostate cancer.

(A) Bone metastasis cases in metastatic prostate cancer patients analyzed through prospective and retrospective investigations [The Metastatic Prostate Cancer (MPC) project, <http://mpcproject.org/>]. (B) Survival rate of prostate cancer patients according to SRC expression (left) and hazard ratios of SRC family kinases (right). Data were obtained from the GEPIA public database. (C, D) Effects of SRC inhibitors on transwell migration and proliferation of metastatic prostate cancer cells. (E) Changes in SRC, FAK, and paxillin activation in prostate cancer cells following treatment with SRC inhibitors. (F) Changes in SRC, FAK, and paxillin activation in osteosarcoma cells treated with SRC inhibitors. (G) Representative confocal images of prostate cancer cells treated with vehicle or SRC inhibitors, showing F-actin-rich invadopodia structures. Cells were stained with phalloidin (green) to visualize F-actin and DAPI (blue) to label nuclei. Arrowheads indicate invadopodia-like actin puncta. Z-stack reconstruction with orthogonal projections and surface plots is shown to visualize the spatial organization, vertical distribution, and relative intensity of F-actin

structures in control and SRC inhibitor-treated cells. All data were presented as mean with SD. Statistical significance of the differences was determined by one-way ANOVA followed by Tukey's test. * $p < 0.05$, ** $p < 0.01$, *** $p < 0.001$, significant difference between indicated points.

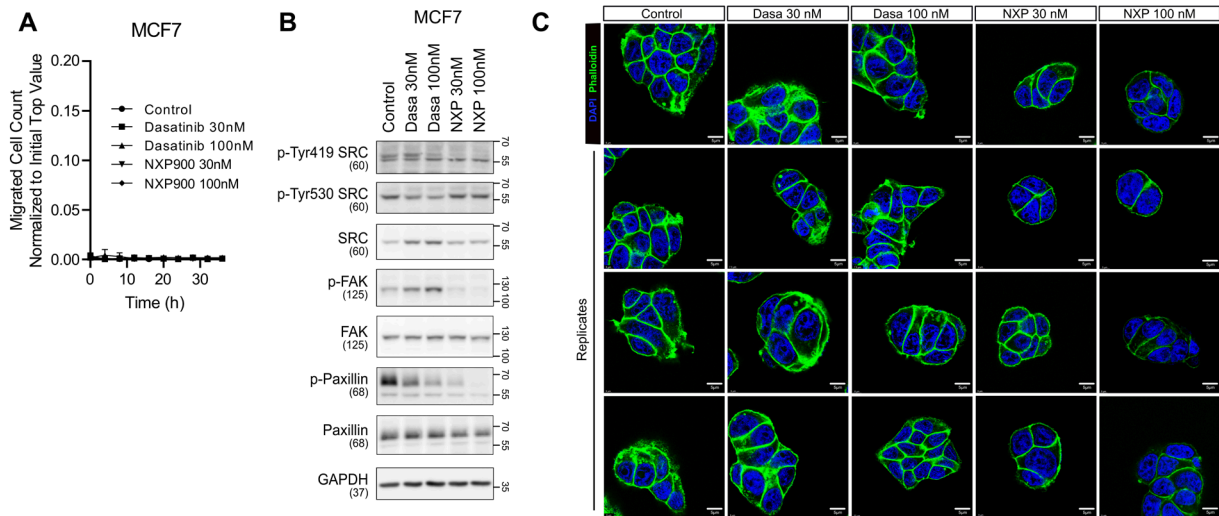


Figure S3, related to Figure 1-2. SRC inhibition suppresses SRC–paxillin–F-actin signaling in ER-positive breast cancer.

(A) Effects of SRC inhibitors on transwell migration of ER-positive human breast cancer cells. (B) Changes in SRC, FAK, and paxillin activation in ER-positive human breast cancer cells following treatment with SRC inhibitors. (C) Representative confocal images of ER-positive human breast cancer cells treated with vehicle or SRC inhibitors, showing F-actin. Cells were stained with phalloidin (green) to visualize F-actin and DAPI (blue) to label nuclei.

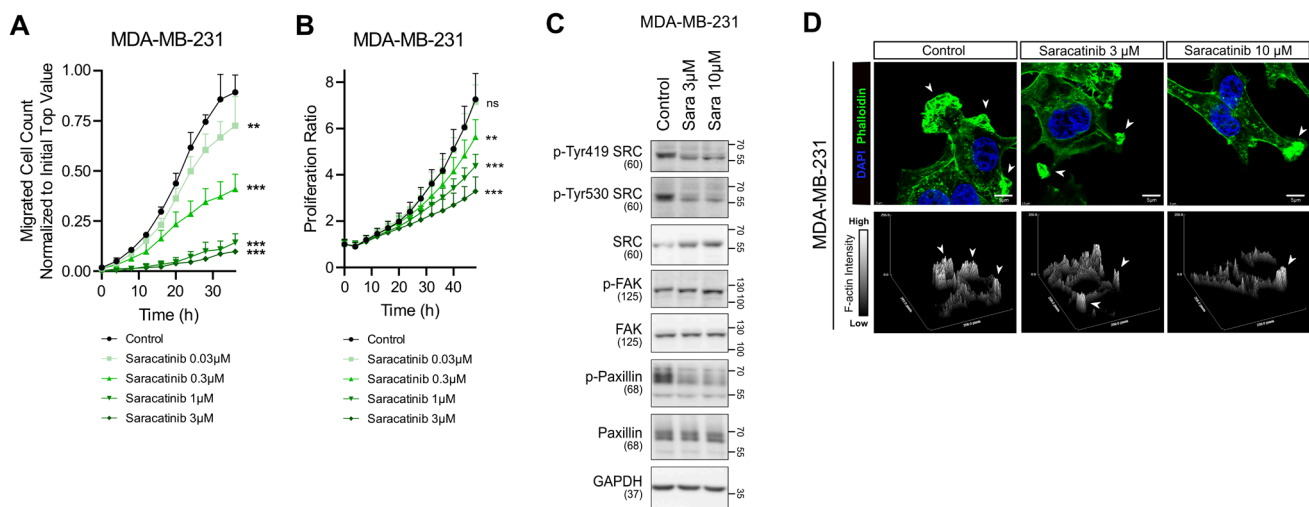


Figure S4, related to Figure 1-2. Validation of SRC-dependent signaling using a conventional SRC inhibitor, Saracatinib.

(A, B) Effects of Saracatinib on transwell migration and proliferation of metastatic breast cancer cells. (C) Changes in SRC, FAK, and paxillin activation in metastatic breast cancer cells following treatment with Saracatinib. (D) Representative confocal images of prostate cancer cells treated with vehicle or Saracatinib, showing F-actin-rich invadopodia structures. Cells were stained with phalloidin (green) to visualize F-actin and DAPI (blue) to label nuclei. Arrowheads indicate invadopodia-like actin puncta. Z-stack reconstruction with orthogonal projections and surface plots is shown to visualize the spatial organization, vertical distribution, and relative intensity of F-actin structures in control and SRC inhibitor-treated cells. All data were presented as mean with SD. Statistical significance of the differences was determined by one-way ANOVA followed by Tukey's test. * $p < 0.05$, ** $p < 0.01$, *** $p < 0.001$, significant difference between indicated points.

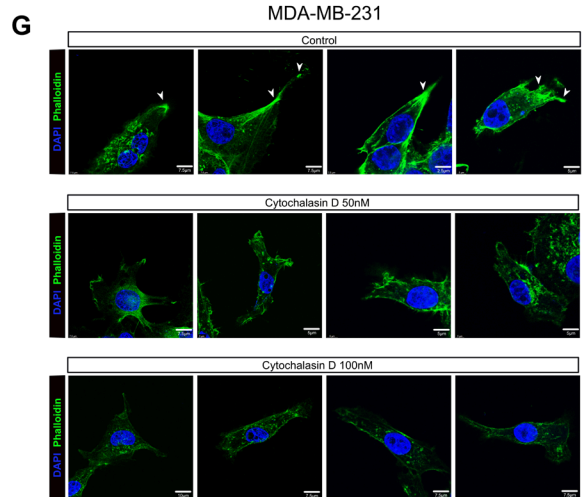
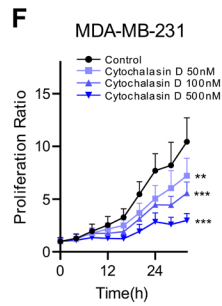
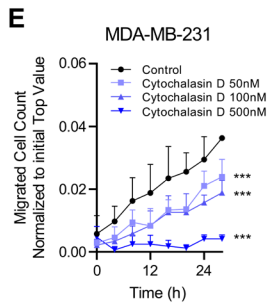
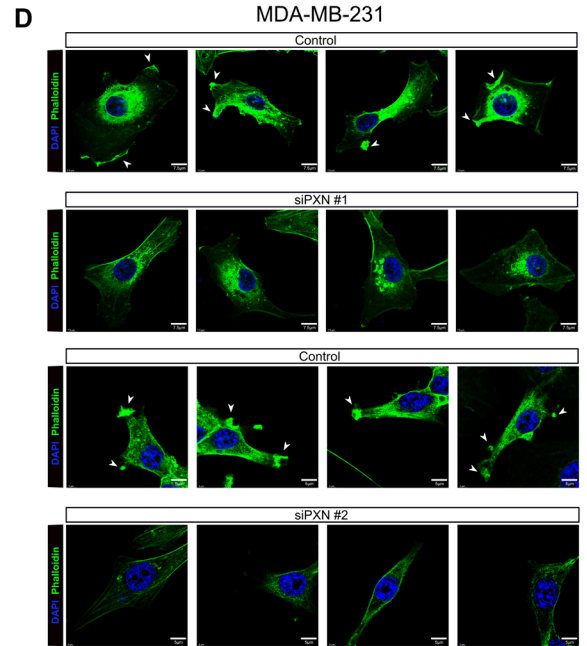
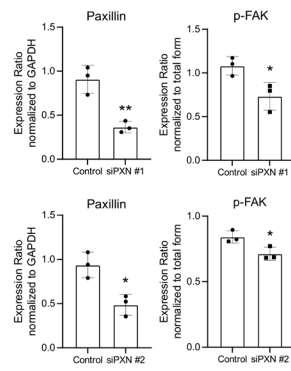
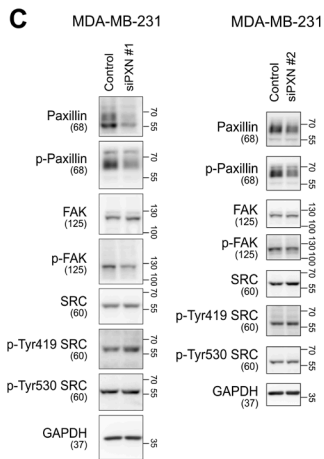
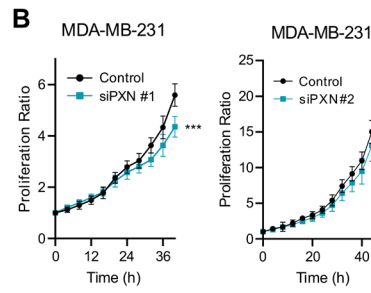
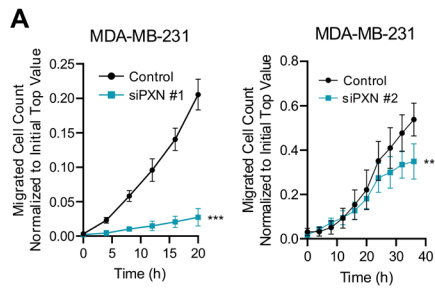


Figure S5, related to Figure 2. Validation of the link between paxillin-mediated actin polymerization and cell motility.

(A, B) Changes in transwell migration and proliferation of breast cancer cells following paxillin knockdown. (C) Alterations in the activation of paxillin, FAK, and SRC after paxillin knockdown. (D) Representative confocal images of breast cancer cells following paxillin knockdown, showing F-actin–rich invadopodia structures. (E, F) Effects of cytochalasin D on transwell migration and proliferation of breast cancer cells. (G) Representative confocal images of breast cancer cells treated with vehicle or SRC inhibitors, showing F-actin–rich invadopodia structures. Cells were stained with phalloidin (green) to visualize F-actin and DAPI (blue) to label nuclei. Arrowheads indicate invadopodia-like actin puncta. All data were presented as mean with SD. Statistical significance of the differences was determined by two-tailed Student's t-test or one-way ANOVA followed by Tukey's test. * $p < 0.05$, ** $p < 0.01$, *** $p < 0.001$, significant difference between indicated points. Detailed information on individual siRNAs is provided in the Methods section.

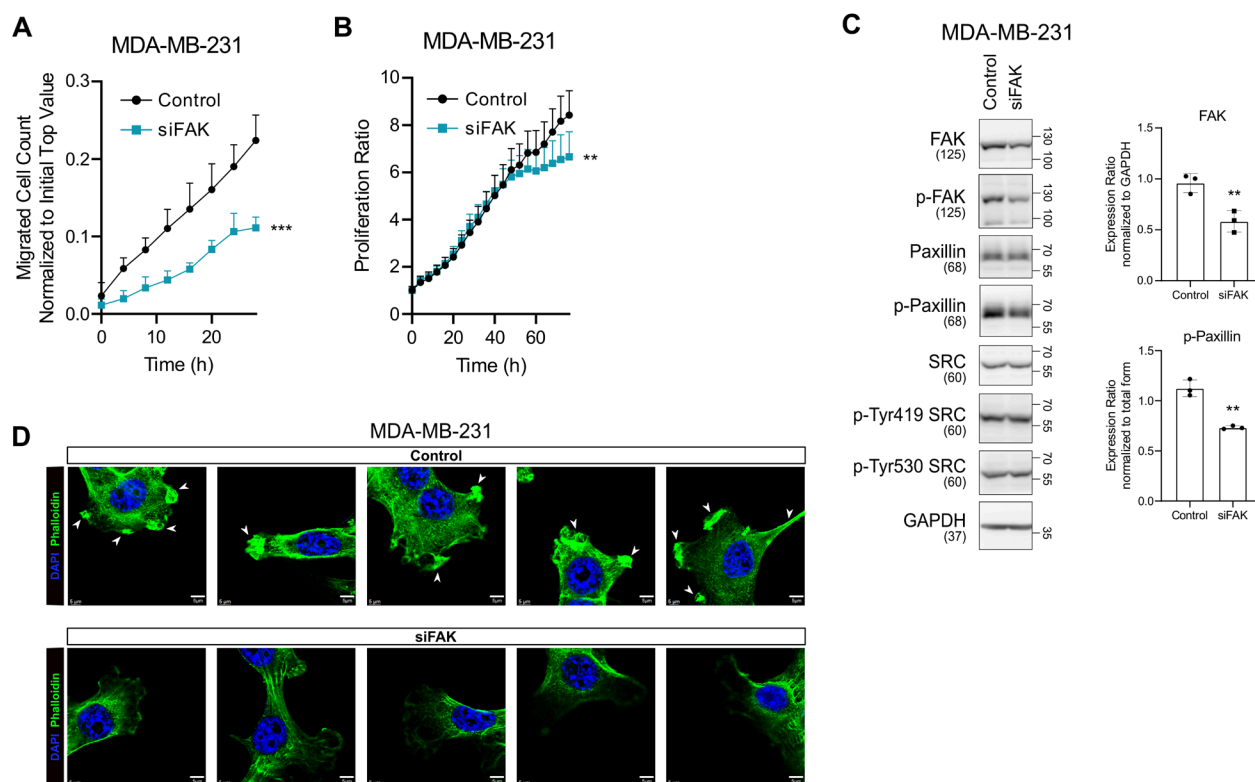


Figure S6, related to Figure 2. Role of FAK in SRC-mediated regulation of cell motility.

(A, B) Changes in transwell migration and proliferation of breast cancer cells following FAK knockdown. (C) Alterations in the activation of paxillin, FAK, and SRC after FAK knockdown. (D) Representative confocal images of breast cancer cells following FAK knockdown, showing F-actin-rich invadopodia structures. All data were presented as mean with SD. Statistical significance of the differences was determined by two-tailed Student's t-test. * $p < 0.05$, ** $p < 0.01$, *** $p < 0.001$, significant difference between indicated points. Detailed information on individual siRNAs is provided in the Methods section.

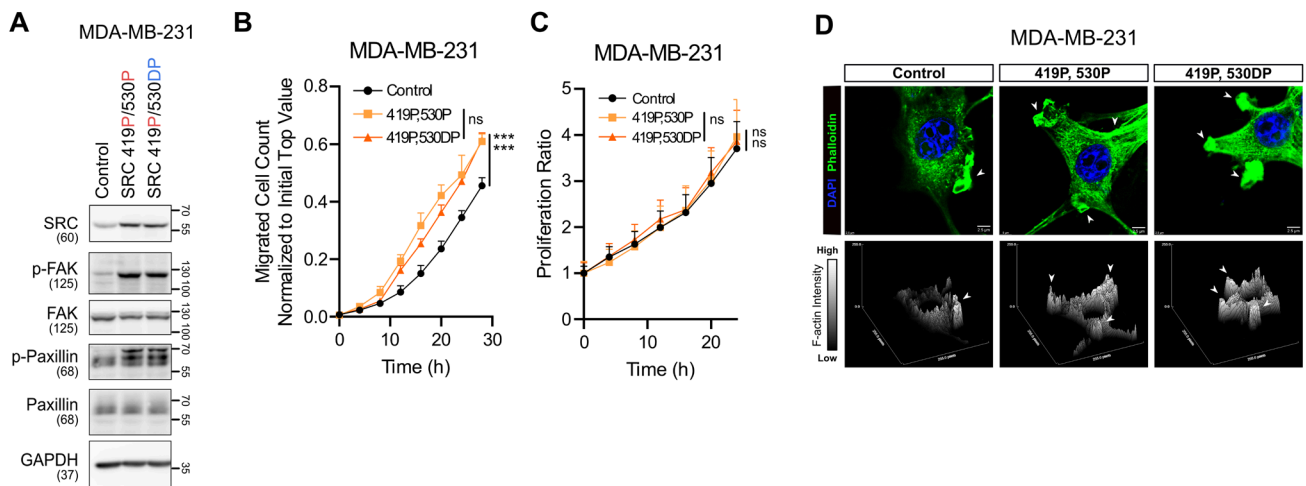


Figure S7, related to Figure 3. Validation of phosphorylation-dependent SRC signaling.

(A) Changes in FAK, and paxillin activation following phospho-mutant SRC plasmids overexpression. (B, C) Changes in transwell migration and proliferation of breast cancer cells following phospho-mutant SRC plasmids overexpression. (D) Representative confocal images of MDA-MB-231 breast cancer cells expressing SRC phospho-mutant constructs (419P/530P, 419P/530DP), showing F-actin-rich invadopodia-like structures. Cells were stained with phalloidin (green) to visualize F-actin and DAPI (blue) to label nuclei. Arrowheads indicate invadopodia-like actin puncta. Z-stack images were reconstructed and displayed as surface plots to visualize the spatial organization, vertical distribution, and relative intensity of F-actin signals across the indicated SRC phospho-mutant conditions. All data were presented as mean with SD. Statistical significance of the differences was determined by one-way ANOVA followed by Tukey's test. * $p < 0.05$, ** $p < 0.01$, *** $p < 0.001$, significant difference between indicated points.

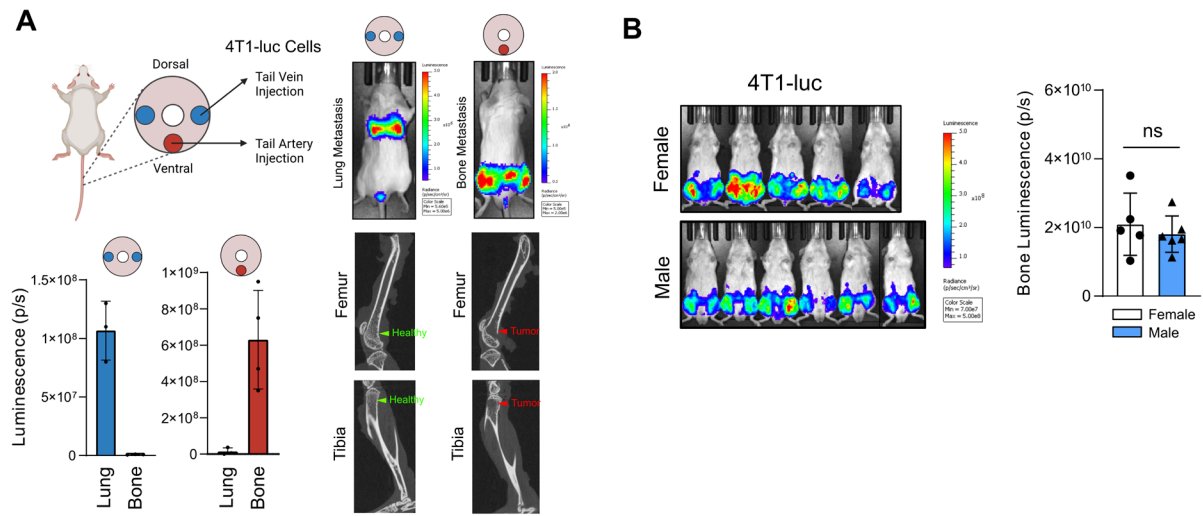


Figure S8, related to Figure 4. Organ-specific metastasis models and sex-dependent effects.

(A) Establishment of bone and lung metastasis models using murine metastatic breast cancer cells. Quantitative assessment was performed using IVIS Spectrum imaging, and qualitative bone evaluation was conducted by micro-CT. (B) Evaluation of sex-dependent differences in breast cancer bone metastasis. Female and male mice were injected with 4T1-luc cells, and metastatic burden was quantified 1 week after injection. N = 5-6/group. All data were presented as mean with SD. Statistical significance of the differences was determined by two-tailed Student's t-test. * $p < 0.05$, ** $p < 0.01$, *** $p < 0.001$, significant difference between indicated points.

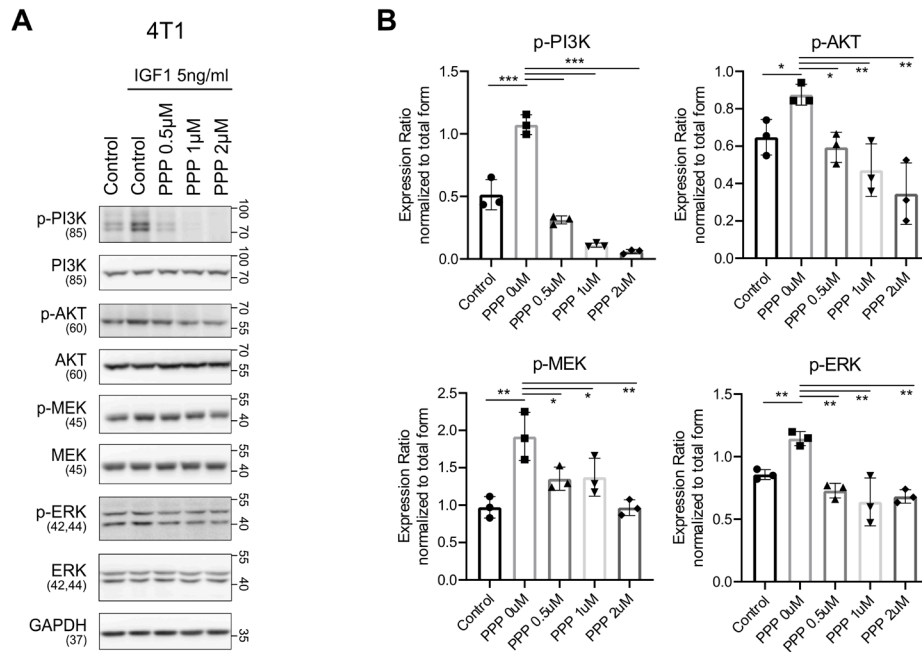


Figure S9, related to Figure 4. Inhibition of IGF-induced tumor growth signaling by picropodophyllin (PPP).

(A) Assessment of IGF-dependent PI3K–AKT and RAS signaling in breast cancer cells following picropodophyllin (PPP) treatment. (B) Densitometric quantification of Western blot results. All data were presented as mean with SD. Statistical significance of the differences was determined by two-tailed Student’s t-test or one-way ANOVA followed by Tukey’s test. * $p < 0.05$, ** $p < 0.01$, *** $p < 0.001$, significant difference between indicated points.

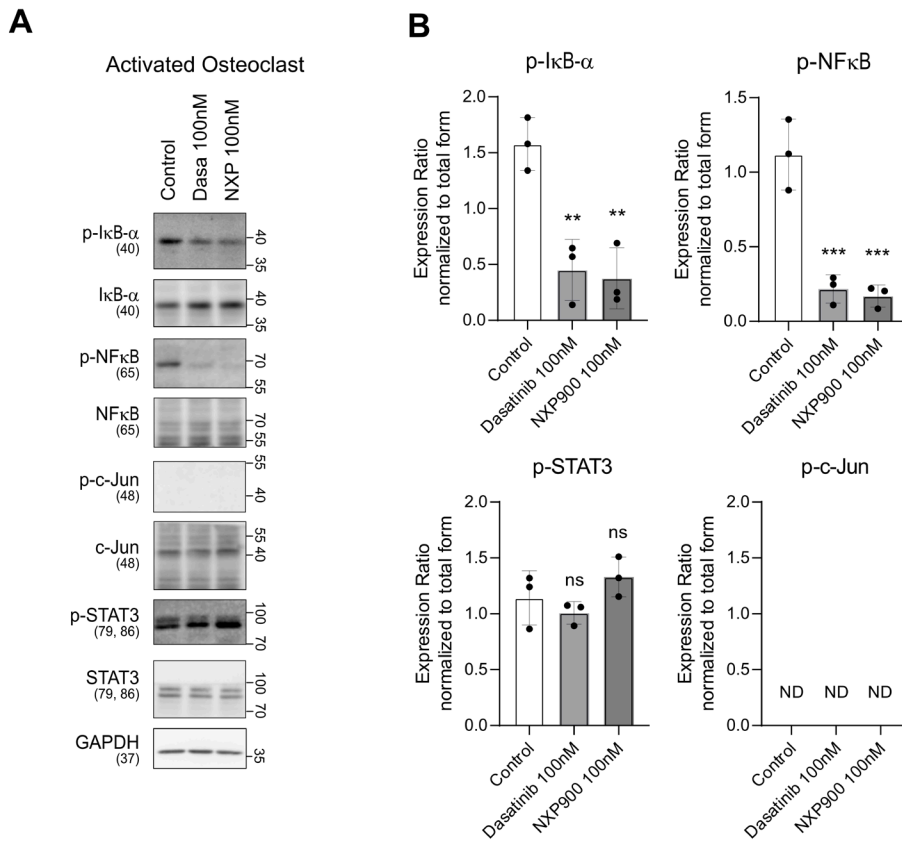


Figure S10, related to Figure 4. SRC inhibition modulates transcription factors associated with osteoclast activation.

(A) Assessment of STAT3, NF-κB, and c-Jun expression in mouse primary osteoclasts following SRC inhibitors treatment. (B) Densitometric quantification of Western blot results. All data were presented as mean with SD. Statistical significance of the differences was determined by one-way ANOVA followed by Tukey's test. * $p < 0.05$, ** $p < 0.01$, *** $p < 0.001$, significant difference between indicated points.

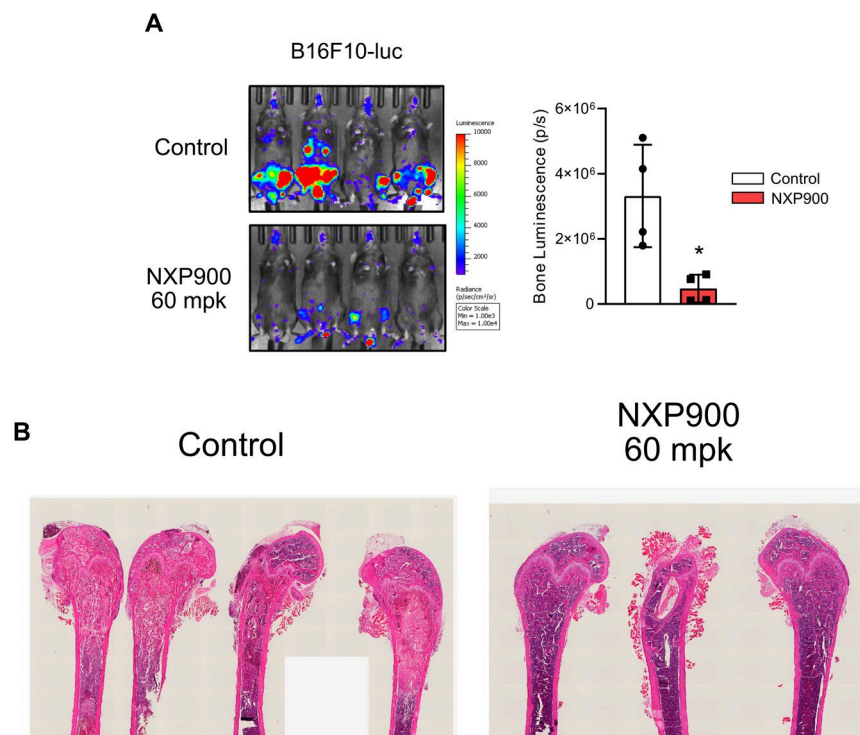


Figure S11, related to Figure 5. Efficacy of NXP900 across different metastatic solid tumor model.

(A) Evaluation of the effect of NXP900 on bone metastasis using the B16F10-luc murine metastatic melanoma cancer model. NXP900 was orally administered daily at 60 mg/kg for 7 days. N = 4/group. (B) Assessment of bone metastatic lesions by H&E staining. All data were presented as mean with SD. Statistical significance of the differences was determined by two-tailed Student's t-test. * $p < 0.05$, ** $p < 0.01$, *** $p < 0.001$, significant difference between indicated points.

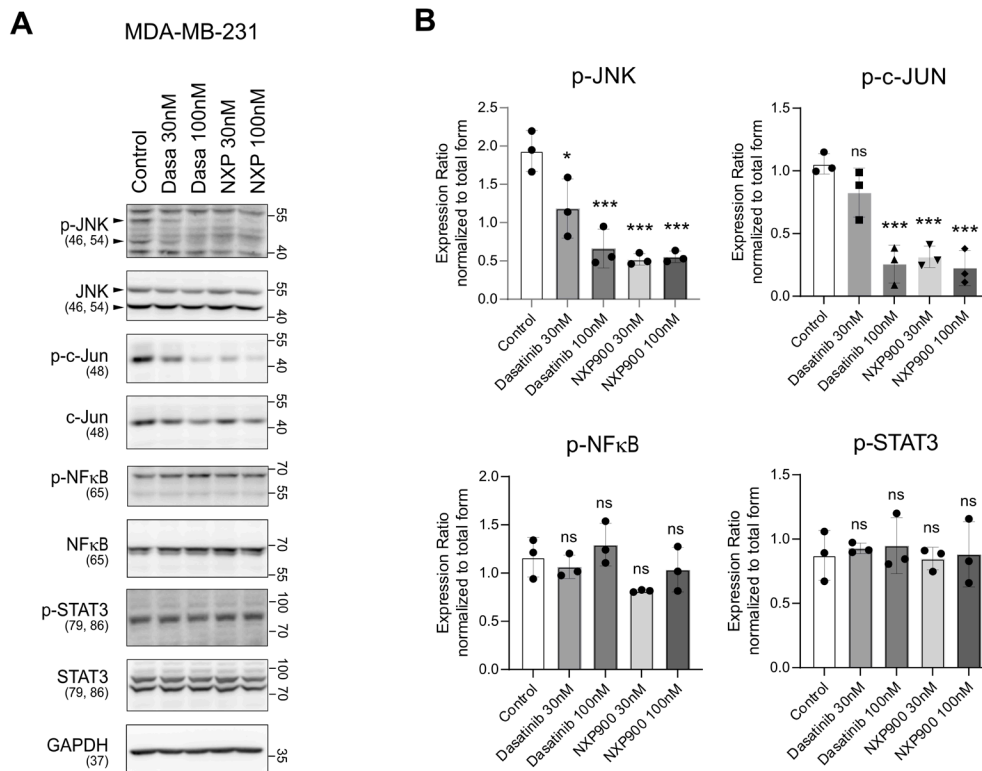


Figure S12, related to Figure 6. SRC inhibition regulates transcription factors associated with PD-L1 expression.

(A) Assessment of transcription factor level regulating PD-L1 in breast cancer cells following SRC inhibitors treatment. (B) Densitometric quantification of Western blot results. All data were presented as mean with SD. Statistical significance of the differences was determined by one-way ANOVA followed by Tukey's test. * $p < 0.05$, ** $p < 0.01$, *** $p < 0.001$, significant difference between indicated points.

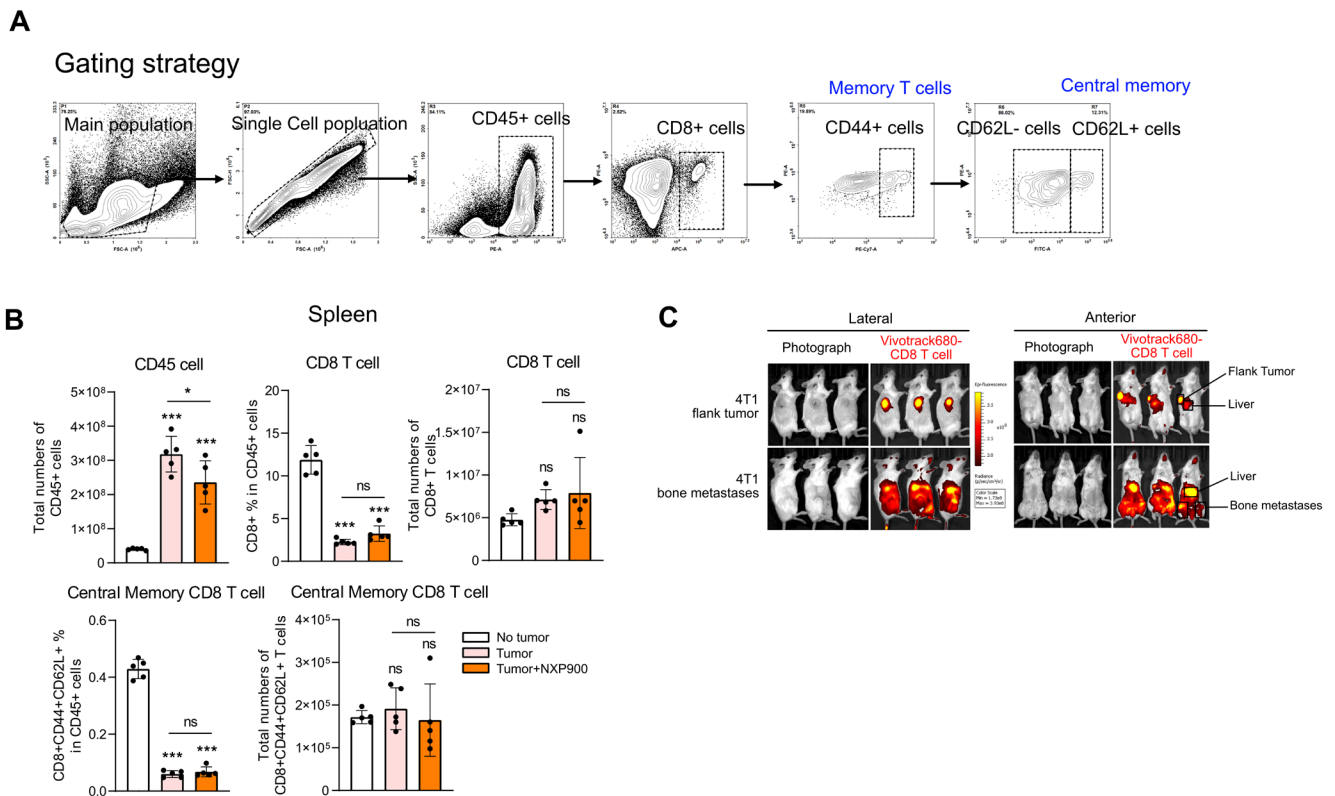


Figure S13, related to Figure 6. Induction of CD8⁺ memory T-cell formation by NXP900 treatment.

(A) Gating strategy used for the analysis shown in Figure 6I and 6J. (B) Quantification of central memory CD8⁺ T cells in the spleen following NXP900 treatment. Absolute immune cell numbers represent counts from a whole spleen. The same samples were used as in Figure 6I. N = 5/group. (C) Validation of tumor-targeting capacity of isolated central memory CD8⁺ T cells. Purified CD8 T cells were labeled with VivoTrack680 and tracked *in vivo* after transfer. All data were presented as mean with SD. Statistical significance of the differences was determined by one-way ANOVA followed by Tukey's test. *p < 0.05, **p < 0.01, ***p < 0.001, significant difference between indicated points.

Table S1. The used cell lines and their respective culture methods.

DMEM: Dulbecco's modified Eagle's medium

FBS: Fetal bovine serum, Thermo Fisher Scientific, Waltham, MA, USA

P/S: penicillin/streptomycin, Hyclone, Logan, UT, USA

Cell line	Culture Medium
4T1	RPMI-1640 medium + 10% FBS + 1% P/S
4T1-luc	RPMI-1640 medium + 10% FBS + 1% P/S
B16F10-luc	High glucose DMEM medium + 10% FBS + 1% P/S
HEK-293T	High glucose DMEM medium + 10% FBS + 1% P/S
MCF-7	High glucose DMEM medium + 10% FBS + 1% P/S
MDA-MB-231	High glucose DMEM medium + 10% FBS + 1% P/S
PC-3	RPMI-1640 medium + 10% FBS + 1% P/S
MG-63	High glucose DMEM medium + 10% FBS + 1% P/S
U2-OS	High glucose DMEM medium + 10% FBS + 1% P/S

Table S2. The used antibodies.**Antibodies for western blotting**

Name	Company	Cat No.
COX-2	Abcam (Cambridge, UK)	Ab15191
Arginase-1	Santa Cruz Biotechnology (Dallas, TX, USA)	sc-271430
PD-L1 (human)	Cell Signaling Technology (Danvers, MA, USA)	13684T
PD-L1 (mouse)	Cell Signaling Technology	60475T
GAPDH	Merck Millipore (Burlington, MA, USA)	CB1001
Phospho-SRC Y416	Cell Signaling Technology	2101s
Phospho-SRC Y530	Cell Signaling Technology	2105s
SRC	Cell Signaling Technology	2108s
p-FAK	Cell Signaling Technology	3283s
FAK	Merck Millipore	05-537
p-Paxillin	Cell Signaling Technology	69363s
Paxillin	Cell Signaling Technology	2542s
MMP-9	Cell Signaling Technology	24317T
N-Cadherin	BD Biosciences (Franklin Lakes, NJ, USA)	610920
E-Cadherin	BD Biosciences	610181
α-Actinin	Proteintech (Rosemont, IL, USA)	66895-1-Ig
Cortactin	Cell Signaling Technology	3503s
Phospho-Cortactin	Cell Signaling Technology	4569s
LIMK1	Proteintech	67974-1-Ig
p-LIMK1/2	Merck Millipore	07-850
Cofilin	Santa Cruz Biotechnology	sc-376476
p-Cofilin	Santa Cruz Biotechnology	sc-271921
Cathepsin K	Santa Cruz Biotechnology	sc-48353

TRAP/ACP5	Santa Cruz Biotechnology	sc-376875
Cyclin B1	Santa Cruz Biotechnology	sc-245
Cyclin D1	Cell Signaling Technology	2922s
p-PI3K	Cell Signaling Technology	17366T
PI3K	Cell Signaling Technology	4257T
p-AKT	Cell Signaling Technology	9271s
AKT	Cell Signaling Technology	9272s
p-MEK	Cell Signaling Technology	9154s
MEK	Cell Signaling Technology	8727s
p-ERK	Cell Signaling Technology	9101s
ERK	Cell Signaling Technology	9102s
p-JNK	Cell Signaling Technology	9251s
JNK	Cell Signaling Technology	9252T
p-c-Jun	Cell Signaling Technology	9261s
c-Jun	Santa Cruz Biotechnology	sc-1694
p-NFκB	Cell Signaling Technology	3033s
NFκB	Santa Cruz Biotechnology	sc-8008
p-STAT3	Cell Signaling Technology	9131s
STAT3	Cell Signaling Technology	4904s
p-IκB-α	Cell Signaling Technology	2859s
IκB-α	Cell Signaling Technology	9242s
HRP-linked anti-rabbit IgG	Cell Signaling Technology	7074s
HRP-linked anti-mouse IgG	Cell Signaling Technology	7076s

Antibodies for flow cytometry

Name	Company	Cat No.
PE anti-mouse MMP9	Santa Cruz Biotechnology	sc-13520 PE
APC anti-human PD-L1		329707
APC anti-mouse PD-L1		124311
PE-Cy7 anti-mouse F4/80		123114
APC-Cy7 anti-mouse CD86		105030
PE anti-mouse CD206	Biolegend (San Diego, CA, USA)	141705
PE anti-mouse CD45		103105
APC anti-mouse CD8		100711
PE-Cy7 anti-mouse CD44		103029
FITC anti-mouse CD62L		104405

Table S3. The used drugs.

Name	Company	Cat No.
NXP900 (eCF506)	TargetMol (Boston, MA, USA)	T8499
Dasatinib	MedChemExpress (Monmouth Junction, NJ, USA)	HY-10181
Saracatinib	MedChemExpress	HY-10234
Cytochalasin D	Thermo Fisher Scientific (Waltham, MA, USA)	PHZ1063
Picropodophyllin	MedChemExpress	HY-15494
Mouse IGF-1 recombinant protein	Thermo Fisher Scientific	250-19-50UG
Gemcitabine	MedChemExpress	HY-17026
Zoledronate	MedChemExpress	HY-13777
Anti-mouse PD-1 antibody	BioXCell (Lebanon, NH, USA)	BE0146